Energy Landscape of the Charge Transfer Reaction at the Complex Li/SEI/Electrolyte Interface

Journal:	*Energy & Environmental Science*
Manuscript ID	EE-ART-12-2018-003586.R2
Article Type:	Paper
Date Submitted by the Author:	25-Feb-2019
Complete List of Authors:	Li, Yunsong; Michigan State University, Chemical Engineering and Materials Science Qi, Yue; Michigan State University, Chemical Engineering and Materials Science

Submitted to EES

Energy Landscape of the Charge Transfer Reaction at the Complex Li/SEI/Electrolyte Interface

Yunsong Li and Yue Qi*

Department of Chemical Engineering and Materials Science, Michigan State University, East Lansing, MI 48824, USA

Abstract

The charge transfer reaction is the fundamental reaction for rechargeable batteries. The energy landscape of this reaction depicts the equilibrium and kinetics of the electrochemical process. Typically, a Li-metal electrode is always covered by a thin layer of solid electrolyte interphase (SEI), forming a complex Li/SEI/electrolyte interface. In this paper, a new modeling framework was developed to predict the energy landscape of the lithiation/delithiation charge transfer reaction at a Li/Li_2CO_3/EC-electrolyte interface, with combined density functional theory (DFT) and tight-binding (DFTB) calculations. It was found that Li^+ ion is much more energetically favorable to be dissolved in the electrolyte on a zero-charged Li-metal electrode, indicating the SEI is a necessary kinetic barrier to prevent complete solvation of Li-metal into the electrolyte. During delithiation, Li^+-ion would be stripped from the surface non-uniformly and form a large void on the Li-metal surface. During lithiation, it was demonstrated the annihilation of Li^+ ion and electron is at the Li/SEI interface, for an idealized defect free SEI. Furthermore, at the experimentally defined zero voltage for Li^+/Li^0, the Li-metal surface is not zero-charged, but rather negatively charged ($\sim 0.62 \pm 0.12$ e nm^{-2}) to maintain the electrochemical equilibrium. The electric field created by the negatively charged surface can reorient the electrolyte into an ordered structure, lower the Li^+ ion desolvation energy barrier, and help the Li^+ ion transport through the SEI. The charge transfer coefficient, α, in the Butler-Volmer equation was directly computed to be ~0.22 from the simulated energy landscape, consistent with the experimental measurements. Thus, this model enables a bottom-up multiscale modeling approach for ion-transfer electrochemical reactions.

*Corresponding Author, Email: yueqi@egr.msu.edu; Tel: 5178892479

1. Introduction

The reversible charge transfer reaction, $M^{z+}(sol) + ze^{-}(s) \leftrightarrow M^{0}(s)$ is the fundamental reaction for rechargeable batteries, where M^0 represents a virtually neutral metal specie, which can be a metal atom or an ion-electron-pair intercalated in an electrode.[1] Simply considering $M^0(s)$ as a metal piece, the forward reaction also describes the electrodeposition process, which can generate mirror like Ag surface [2] or mossy and dendritic Li that is harmful to battery life and safety. [3-5] The backward depletion reaction is the source for many corrosion processes. [6] The energy landscape of this reaction, with broad applications, depicts the equilibrium and kinetics of the electrochemical reaction, which is often phenomenologically described by the Butler-Volmer equation. [7-9]

Predicting the charge transfer reaction energetics from first-principles calculations, such as density functional theory (DFT), is necessary for achieving interface design. It is especially valuable for the fundamental electrochemical reactions taking place at complex interfaces, where microscopic structural and chemical properties are often difficult to probe under operating conditions. Recently, various methods have been developed, including joining DFT with implicit continuum solvation model,[10, 11] using DFT for explicit electrode/electrolyte solvents model, [12] and constraining electrons to capture electron hopping by the constrained-DFT model. [13] Most of these electrochemical reaction simulations dealt with pristine-metal/aqueous interfaces; [14-16] where the catalyst metal surface is neither the product nor the reactants of the electrochemical reaction. Currently, modeling of the energy change for the metal deposition type of charge transfer reaction is not available, despite its broad applications.

For many electrochemical interfaces, the metal surface is not pristine. [17] The application of Li-metal-electrode in batteries amplifies the effect of the surface passivation layer. The typical non-aqueous electrolytes are thermodynamically unstable against reduction reactions on the surface of typical negative electrodes, leading to organic and inorganic components depositing on the electrode surface to form a passivation layer, which is often referred as the solid electrolyte interphase (SEI).[18-20] The Li^+ conducting and electronically insulating SEI can prevent further electrolyte reduction and lithium consumption during cycling.[21] Therefore two important charge transfer reactions can occur at the complex Li/SEI/electrolyte interface. The first one is the desired *ion transfer* reaction occurring in each charge/discharge cycle, $Li^+ + e^- \leftrightarrow Li^0$. The others are a series of undesired *electron transfer* reactions leading to electrolyte decomposition. While most modeling work focused on the latter by simulating electrolyte reduction reactions on zero charged

pristine or SEI-covered negative electrodes, [22-24] the first one deserves equal attention as it is essential for a comprehensive description of charge/discharge processes in developing stable and efficient Li-ion batteries. [25-28]

Predicting the energy landscape of the electrochemical reaction of $Li^+ + e^- \leftrightarrow Li^0$ at the complex Li/SEI/electrolyte interface faces several computational challenges. First, it requires electronic structure calculations for a large interface structure that is beyond the size of typical quantum calculations. Fortunately, for the *ion diffusion* reaction, the excited and confined electronic states controlling electron transfer in the Marcus theory can be neglected, so traditional DFT and even self-consistent charge density functional tight-binding (SCC-DFTB) method can be adequate.[29, 30] Therefore, in this study, a new half-cell interface model containing a Li-metal, covered by 4 layers of Li_2CO_3 and interfaced with liquid ethylene carbonate (EC), was created as an explicit electrochemical model to represent the Li/SEI/electrolyte interface. Although the model seems to be over simplified for the multicomponent SEI, considering previous simulations on SEI component, such as Li_2CO_3, LiF, $(CH_2OCO_2Li)_2$ have led to many important and experimentally verified predictions on SEI functionality (summarized in Ref 23), it can be expected this model, as a first step toward predicting charge transfer reactions at a complex interface, will lead to new insights. This explicit half-cell model is motivated by the Li-symmetric cells that reach electrochemical equilibrium in an enclosed system. It facilitates the simulation of reduced state and oxidized states. SCC-DFTB with new parameters transferrable to Li^+ ion and Li^0 metal [31] was used to capture the dynamics of the liquid-electrolyte, the charge on the electrode, and the average system energy, while DFT was used occasionally to freeze the half-cell structure and calibrate the SCC-DFTB results. Together, the energy landscape for the fundamental charge transfer reaction $Li^+ + e^- \leftrightarrow Li^0$ at a complex Li/Li_2CO_3/liquid-EC-electrolyte interface was obtained.

It is still computational challenging to predict various potentials defined in electrochemistry and applying an over-potential, η, to drive the electrochemical reaction. In this work, we first derived the thermodynamic driving force and defined the electrochemical equilibrium conditions ($\eta = 0$) for the charge transfer reaction with the explicit half-cell interface model from both DFTB and DFT calculations. The definition of the voltage in the explicit model is inspired by the interface model for a LiC_6/liquid-EC interface (no SEI), where the surface electron density (σ) on LiC_6 was calibrated to mimic an experimentally-defined applied voltage.[24, 32] It is important to note that at $\eta = 0$, the experimentally defined zero voltage for Li^+/Li^0, the Li-metal surface is

negatively charged. As simulations with classical force field have indicated that the electric field created by the negatively charged surface can and change the electrolyte double layer structure [33], [34, 35] the explicit half-cell interface model developed in the study will fully illustrate the energy landscape variation under different electric field, which is connected to the excess electron density on the Li-metal-electrode. Thus, the de-solvation energy barrier, the double layer structure, and the Li^+ ion transport barrier through the SEI were predicted as a function of the over-potential. Finally, the charge transfer coefficient, α, in the Butler-Volmer equation was directly predicted from the computed energy landscape.

2. Simulations of the Electrochemical Reaction with a Half-Cell Interface Model

The half reaction at the Li/SEI/electrolyte interface can be written as

$$Li^+(sol) + e^-(s) \leftrightarrow Li^0(\mathrm{s}) \quad (1),$$

where the Li^+ ions dissolved in the electrolyte are reduced by the electrons, e^-, on the electrode to produce the Li^0 atoms depositing to the Li-metal electrode (forwarding reaction). The thermodynamic driving force is given by

$$\Delta G = \Delta G^0 + F\phi - RTlna_{Li^+} \quad (2),$$

where ΔG^0 is the standard free energy change for the electrode reaction (1) on a zero charged Li-metal, F is the Faraday constant. ϕ is the *Galvani* potential on the Li-metal electrode (assuming the potential in the electrolyte to be the zero). a_{Li^+} is the activity of Li^+ ions in the electrolyte, which depends on temperature, solvent, and the concentrations of ions. At the electrochemical equilibrium, the forward and backward currents are equal, or in other word, the chemical potential of Li^+ ions in the electrolyte equals to the chemical potential of a reduced Li^0 atoms in the electrode, thus

$$\Delta G = \Delta G^0 + F\phi^0 - RTlna_{Li^+} = 0 \quad (3),$$

where ϕ^0 is the equilibrium potential. During the charge or discharge process, the thermodynamic driving force for the reaction can also be expressed as,

$$\Delta G = F(\phi - \phi^0) = F\eta \quad (4),$$

where η is the over-potential. If $\eta < 0$, the Li^+ is reduced (plating); whereas if $\eta > 0$, the Li^0 is being oxidized to Li^+ ions (stripping). The energy landscape along the reaction coordinate under different potential is schematically shown in Fig. S1 in the Supporting Information (**SI**). The over-

potential tilts the energy landscape, causing the imbalance of the forward and backward currents, leading to the well-known phenomenological Butler-Volmer Equation.

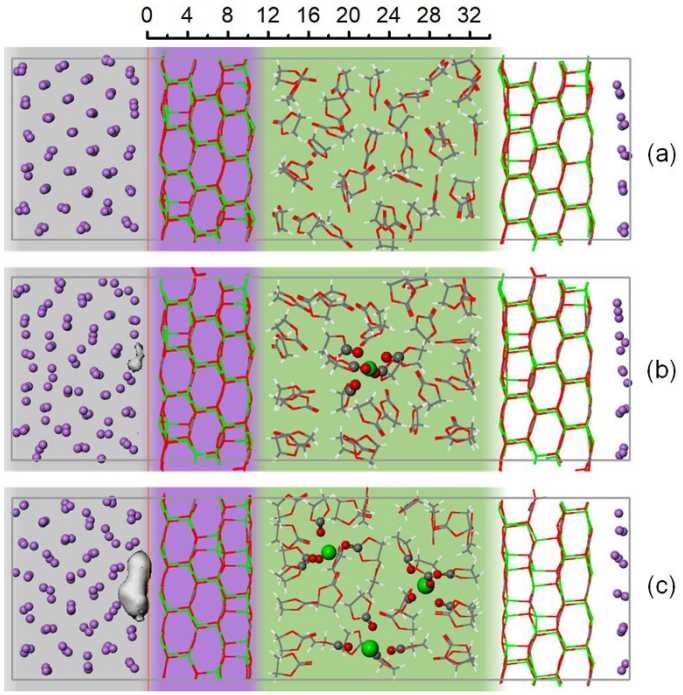

Fig. 1. Li/Li_2CO_3/EC slab models at (a) the reduced state, and at the oxidized states with (b) one Li atom and (c) 3 Li atoms stripped. The white volume in (b) and (c) indicates the location of the stripped Li atoms. The reaction coordinates (RC) of 0 and 12 Å correspond to the position of the Li-metal surface and EC-electrolyte surface, respectively.

In order to understand the Li plating/stripping process at atomistic scale and to directly predict the energy landscape under different over-potential for reaction (1), an explicit half-cell interface model was created in this paper. Here, a Li(001)/Li_2CO_3(001)/liquid-EC slab model [20] was used to represent the Li/SEI/electrolyte interface, as shown in Fig 1. More specifically, the model includes a 7-layer of Li-metal with a thickness of ~11 Å, 4 layers of Li_2CO_3 on each side of the Li-metal with a thickness of ~12 Å, and a thick liquid EC slab including 32 EC molecular with an experimental density of 1.32 g cm^{-3}. The fully periodic cell has a dimension of 16.72 x 9.95 x 56.91 $Å^3$ and 809 atoms. The average total energy of the simulation cell was obtained from 50ps SCC-DFTB molecular dynamics (MD) simulations. Several snapshots of relaxed SCC-DFTB structures were fully relaxed by DFT (GGA/PBE) again to calibrate the accuracy of the SCC-

DFTB results. More calculation details are listed in the **SI**. It was also found the SCC-DFTB relaxation dramatically accelerated the convergence of the DFT relaxation.

The reduced state is represented by a perfect Li-metal slab and no Li^+ ions in the liquid (as **Fig. 1a**). The oxidized states are represented by removing one (**Fig. 1b**), two, three (**Fig. 1c**) and five Li^+ from the Li-metal slab, respectively, and putting them randomly inside the electrolyte and leaving vacancies in the Li-slab. After minimization, it was found the electrons were left on the Li-metal slab. Our previous study had shown that 4-layer of Li_2CO_3 can kinetically stabilize a negatively charged Li-metal surface for at least 100ps of DFTB MD simulation without reducing EC.[31] The energy landscape for the charge transfer reaction was obtained by moving one Li^+ ion from the center of the electrolyte toward the Li-metal surface. Several special locations were considered, e.g., the center of the electrolyte, the SEI/electrolyte interface, in the Li_2CO_3 layer and on the Li-metal surface. At each location of the Li^+ ion, all the other atoms are fully relaxed by SCC-DFTB or by DFT (GGA/PBE) minimization, expect the Li^+ ion that is moving along the normal direction of the interface. In order to locate where the charge transfer occurs, the electron distribution was computed for the metal slab, the Li_2CO_3, and the Li-ion and the EC electrolyte, by summing the atomic charges in each phase. The atomic charge in DFT was based on Bader charge analyses,[36] while the atomic charge in SCC-DFTB is based on the Mulliken population, implemented in the DFTB+ code (for the convenience of the theory). Based on our interface model, in the oxidized state with one Li^+ in the electrolyte (**Fig 1b**), the Li^+ ion in the electrolyte is +0.62 charged, while the Li-metal slab gained -0.46 charged in SCC-DFTB calculations. DFT predicted the Li^+ ion in the electrolyte to be +1.0 charged while the Li-metal slab is -0.96 charged. Both indicated the electron and ion are separated, while the overall interface model is neutral.

To maintain an overall neutral cell, the Li^+ ion concentration (c_{Li^+}) in the electrolyte increases with the more negative electronic field caused by the excess electrons on Li-electrode. This general phenomena of increasing ion concentration near a charged surface has been observed in SEI covered graphite surface[34] and aqueous NaCl solution[35] with classical MD simulations. Therefore, it is possible to neglect the influence of the neutral background of the electrolyte ($LiPF_6$ dissolved in EC for battery case) and only focus the excess Li^+ ion concentration near the electrode/electrolyte interface, where the excess Li^+ ion concentration is balanced with the excess electrons on the electrode. This assumption is motivated by experimentally used symmetric Li-metal cells, where an electrochemical equilibrium is established in a closed system. With this

closed system, the total excess electrons on the Li-metal slab equals to the total charge of the Li^+ ion in the electrolyte (q_e), as

$$-2\int \sigma dA = k_\sigma c_{Li^+} V = q_e \quad (5),$$

where A is the surface area of Li-metal slab, σ is the excess electron density on Li-metal slab, V is the electrolyte volume, the factor "2" denotes the two surfaces of the slab, and k_σ is introduced to represent the different charged states in SCC-DFTB and DFT calculations, thus k_σ is 0.46 e for SCC-DFTB and 0.96 e for DFT. The electric potential should drop to zero in the center of the liquid EC to mimic the electrolyte out of the Helmholtz layer (at least when Li^+ concentration is not too high). The electric potential drop was calculated from the classical electrical double layer (EDL) model and DFT calculations (**Fig. S2**). These results along with previous MD simulations[34] all suggested that the electric potential will drop to zero within 1nm in the EC electrolyte, confirming that the half-cell interface model is long enough and it can be used to obtain the energetics in a charged system explicitly**.**

III. Results and Discussion

3.1 The equilibrium conditions for the charge transfer reaction

The charge transfer reaction energy on a zero-charge Li-electrode can be evaluated via the thermodynamic cycle illustrated in **Fig. S3** in the **SI**. In this process, a Li atom will be removed from the Li-metal (the vacancy formation energy $E_f(V_{Li})$ = 0.4 eV from DFT calculations) to the gas phase (vaporization energy E_{vap}= 1.4 eV [39], close to the DFT calculated cohesive energy of 1.61 eV), then be ionized (ionization energy of Li, E_{ion}= 5.4 eV [40]). The Li^+ ion will then be dissolved into the electrolyte (solvation energy, $E_{sol}(Li^+)$), while the electron will return to the Li-metal electrode according to the reverse of work function (W_f). Therefore,

$$\Delta G^0 = -E_f(V_{Li}) - E_{vap} - E_{ion} + W_f + E_{sol}(Li^+) \quad (6)$$

The solvation energy was 5.2 eV from the AIMD method with GGA/PBE functional at 450 K,[24] and possibly even lower with entropy cost [41]. It was reported to be 4.4 eV for $Li^+(EC)_4$ from Gaussian with the Hartree-Fock method.[42] In the current simulation, the DFT (with GGA/PBE functional) computed solvation energy with one Li^+ ion surround by 5 EC, mincing the first

solvation shell with a gas phase, is 5.5 eV. [41] The calculated $E_{sol}(Li^+)$ is 5.4 eV using SCC-DFTB MD simulation at 450 K. Therefore $E_{sol}(Li^+)$ =5.5 eV from DFT was used for the thermodynamic cycle calculation. The computed W_f = 2.96 eV from DFT (with GGA/PBE functional) on a zero charged Li-metal slab was also in good agreement with reported experimental or computational data about 2.90-3.10 eV.[43, 44] Therefore the ΔG^0 computed from the thermodynamics cycle in **Eq (8)** is ~1.26 eV. Note **Eq (6)** has an additional vacancy formation term, since a vacancy will be generated during Li depletion, compared to the thermodynamic cycle in Ref,[45] which predicted a reasonable higher ΔG^0 of ~1.5eV. Taking the normal hydrogen electrode (NHE) as a reference ($4.5 \pm 0.2\,V$ at physical scale), [9, 46] the **computed standard electrode potential,** E^0, for Li^+(EC)/Li^0 is $E^0 = \Delta G^0 - \Phi_{NHE} = 1.26 - 4.5 = -3.2 \pm 0.2$ V, which is very close to the reported -3.04 eV for Li^+ ion in aqueous solution.

For reaction (1), a positive ΔG^0, $\Delta G^0 > 0$, means that Li^+ ion is much more energetically favorable to be dissolved in the electrolyte, if the Li-electrode is zero-charged. This is also supported by the spontaneous reactions when a Li-metal is soaked in EC electrolyte from ab initio MD simulations. [24] Therefore the SEI is a necessary kinetic barrier to prevent complete solvation of Li-metal into the electrolyte. The corresponding **electrochemical equilibrium potential** determined directly by **Eq (3)** is $\phi^0 = -\frac{\Delta G^0}{F} \sim -1.26\,V$, assuming the $a_{Li^+} = 1$. This is reasonably lower (should be ~0.1 V lower) than that of a carbon electrode, which is about -1.18 V calculated via DFT with a C-electrode/EC-electrolyte interface model. [24]

Submitted to EES

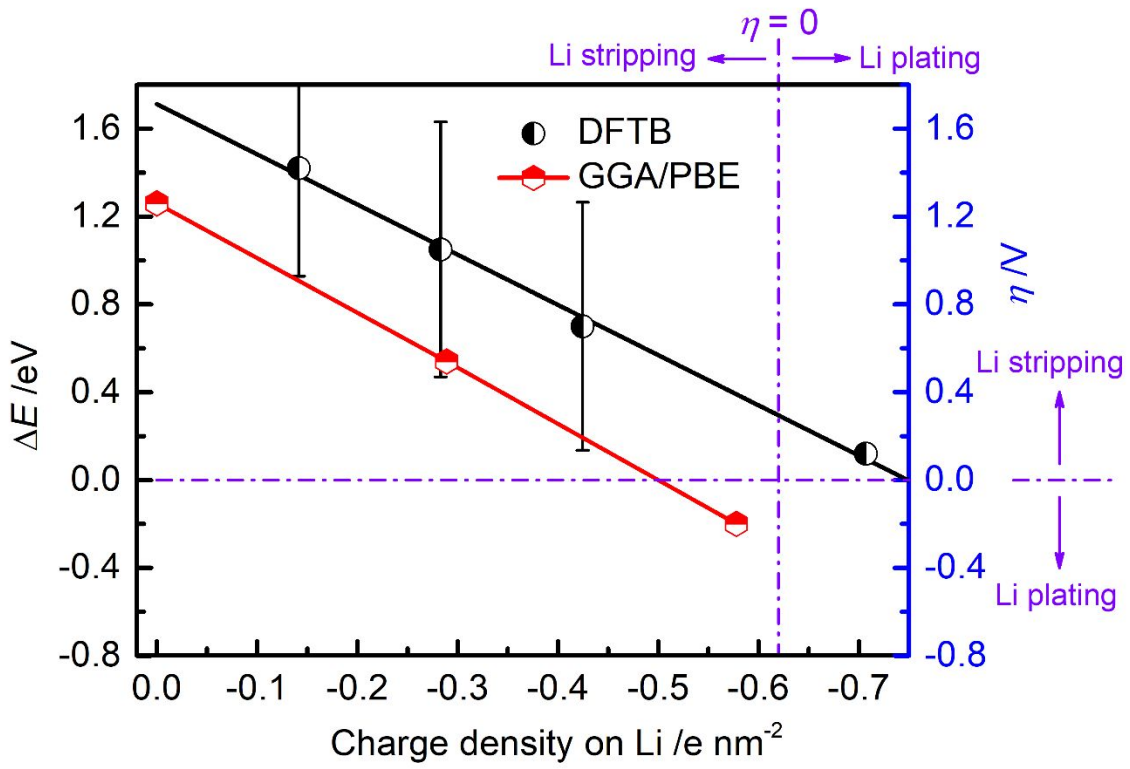

Fig. 2. The electrochemical driving force of the charge transfer reaction at the Li/Li_2CO_3/EC-electrolyte interface as a function of the charge density on the Li-metal surface. The circle and hexagon denote the directly predicated ΔE by SCC-DFTB and DFT, respectively.

Fig. 2 shows the electrochemical reaction driving force (the over-potential) in **Eq (3).** This is the energy difference with respect to ϕ^0 and it is directly computed as the energy difference between the reduced state (e.g. **Fig. 1a**) and oxide states, ΔE, using the half-cell interface model. For the DFT results, the ΔE at the zero-charged Li-metal equals to 1.26 eV obtained from the thermodynamics cycle calculation. Based on both SCC-DFTB and DFT calculations, ΔE decreases with the more negative charge density, σ, on the Li-metal electrode. It reaches zero at the charge density of -0.75 and -0.50 e nm^{-2} from SCC-DFTB and DFT calculations, respectively. The deviation between DFT and SCC-DFTB was induced by approximations of the SCC-DFTB method and parameters.[47] Given the lack of dynamics of DFT simulations and the lack of accuracy of SCC-DFTB results, we estimated the charge density on the Li-metal electrode with the average of both methods as -0.62 ± 0.12 e nm^{-2} at the electrochemical equilibrium state of $\eta = 0$.

As the negative charge on Li-electrode causes Li^+ ion concentration to increase near the surface, we have evaluated the activity change, which is linked to the solution energy change, due to concentration (details are shown in **SI**). The change in the solubility with Li^+ ion concentration increasing from 0.4 M to 2.24 M is less than 0.25 eV. So, the decrease of ΔE is mainly caused by the electric potential shift due to the excess charge density on the Li-metal electrode, which has been estimated by **Eq S(1)** and S**(2)** in **Fig. S2a**. For a charge density of -0.62 e nm^{-2}, the shift is about 1.1 V, consistent with the potential drop observed from the half-cell model.

The **electrochemical equilibrium,** corresponding to the experimentally defined zero voltage of $Li^+|Li^0$ in the EC electrolyte is reached when $\Delta E \sim \Delta G = 0$. This means, the **electrochemical equilibrium potential,** ϕ^0, occurs on a negatively charged Li-metal electrode, not a zero-charged Li-electrode. Even stripping Li atoms from the Li-metal electrode under an applied 1 V over-potential still occurs on a negatively charged Li-metal electrode. This suggested that the Li-metal surface is negatively charged most of the time during stripping and plating cycles. The consequence of the negatively charged Li-metal surface on the ion transport will be discussed in the Sections 3.4~3.6. It should also impact SEI growth dramatically, which is beyond the scope of this study.

3.2 Interface Defects Formation During Li-stripping

It was suspected that Li becomes porous near the surface during delithiation. [48] The half-cell interface model provides a consistent way to illustrate where the Li will be removed from the Li-metal slab. **Fig. 3** shows the relaxed Li/Li_2CO_3 interface structures with the lowest energy from the half-cell model and the cross-section of the Li-surface after 1 Li, 2 Li, and 3 Li atoms were stripped. The highlighted circles mean other possibilities to remove Li. The optimized Li/Li_2CO_3 interface undergoes obvious atomic relaxation. When one Li is removed, a vacancy can be generated either from the surface (case I) or from the bulk (case II) of the Li-metal slab (**Fig. 3a**). The calculated total energy of case I is 0.3 eV lower than that of case II, suggesting Li will be stripped from the surface first. During delithiation, the Li will continuously be removed from the Li-metal slab. The second Li may be removed around (case I) or far away from (case II) the first Li vacancy. The calculated total energy of case I is 0.58eV lower than that of case II, indicating the second Li will be removed around the first Li vacancy. Similarly, the third Li may be removed

around (case I and II) or far away from (case III) the Li vacancy (**Fig. 3c**). The calculated results show that case I is the most stable with the lowest total energy and is 0.32 eV and 0.49 eV lower than that of case II and case III, respectively. Therefore, Li atoms will be stripped from the surface with non-uniformity and prefer to form a large void during delithiation. Considering the low work of adhesion at Li/Li_2CO_3 interface (W_{ad} = 0.167 J m^{-2} for Li(001)/Li_2CO_3(001) and 0.124 J m^{-2} for Li(110)/Li_2CO_3(001) from GGA/PBE,[49] and 0.26 J m^{-2} for Li(001)/Li_2CO_3(001) from our SCC-DFTB calculations), void generation at the interface will likely lead to SEI delamination during delithiation, if a compressive stress is not applied. Also, the void generation at the Li/SEI interface will also impact the morphology of the subsequent lithiation cycle. This may explain why compressive stress is beneficial during Li-stripping and plating experimentally. [50]

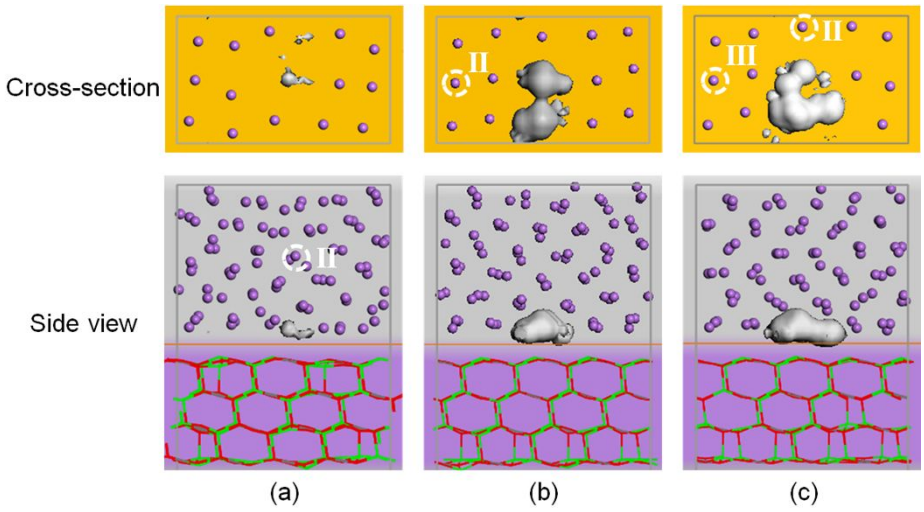

Fig. 3. The relaxed Li/Li_2CO_3 interface structures after (a) 1 Li, (b) 2 Li and (c) 3 Li atoms stripped. The top pictures are the cross-section of the Li-metal surface. The while filled circles indicate the location of Li vacancy, and the dotted circles denote the other considered location of Li vacancy. The while volume indicates the location of the void.

3.3 The charge transfer reaction occurs underneath the perfect SEI

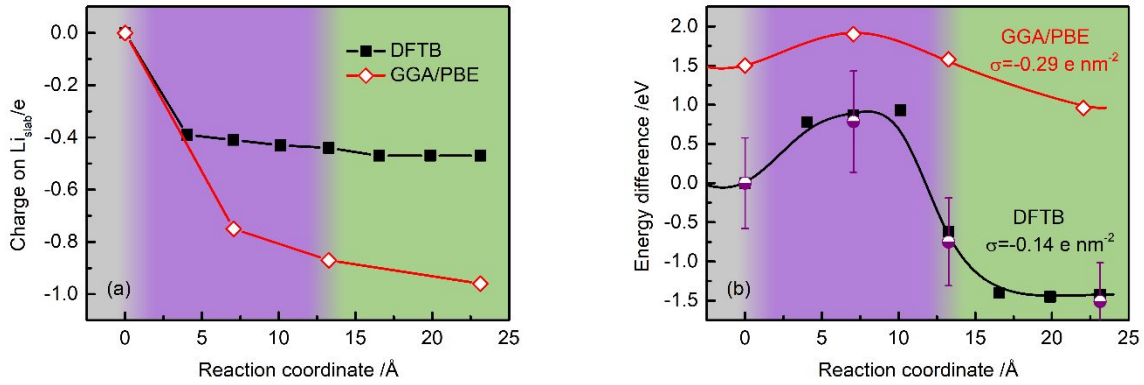

Fig. 4. (a) The calculated total charge on the Li metal slab and (b) the energy variation when one Li^+ ion transports through the EC-electrolyte (green) and the Li_2CO_3 layers (purple) to the surface of Li-metal (gray). The full-filled squares are from SCC-DFTB minimization, the half-filled circles are from SCC-DFTB MD average along with its fluctuation range, and the unfilled diamonds are from DFT calculations.

The interface model allows us to track the charges on the Li-metal slab, electrolyte, and the Li_2CO_3 phases, while the Li^+ ion diffuses from the electrolyte to the Li-metal surface. **Fig. 4a** shows the total charges on the Li-metal electrode when one Li^+ ion is at different locations in the interface cell, indicated by the reaction coordinate as its distance to the Li-metal surface. It shows that the total charges on the Li-metal slab kept almost a constant of -0.46e with the SCC-DFTB method when one Li^+ ion is located in the EC-electrolyte and in the Li_2CO_3 layers. The charge on the Li-metal turned into zero when Li^+ ion reached the Li-metal surface, indicating the annihilation of e^- and Li^+ ion occurs underneath the perfect SEI layer and at the Li-metal surface. In order to verify the SCC-DFTB result, several SCC-DFTB optimization structures were further optimized with DFT and the charge density distribution was evaluated. The DFT predicted total charges on the Li-metal slab were about -0.96e when one Li^+ ion is located in EC-electrolyte, and gradually reduced to -0.78e with Li^+ ion moving inside the Li_2CO_3 layers. The charge on the Li-metal also dropped to zero when Li^+ ion landed on the Li-metal surface. The corresponding electron density on the Li-metal, when Li^+ ion is in the electrolyte, is -0.14 and -0.29 e/nm^2 from SCC-DFTB and DFT calculations, respectively. The charge values from the DFT calculations are almost twice of that from SCC-DFTB, due to the limitation of SCC-DFTB, underestimating the amount of charge transfer. However, both methods show a similar trend of charge variation on the Li-metal slab

when Li^+ ion transports from the EC-electrolyte, through the Li_2CO_3, and lands on the Li-metal surface. Note that this model uses a perfect Li_2CO_3 slab to represent an idealized SEI, and this conclusion may change due to the defects in real SEI.

3.4 The energy landscape of the charge transfer reaction

Fig. 4b shows a representative energy landscape for the charge transfer reaction through the Li/Li_2CO_3/EC-electrolyte interface model. This is the total energy of the half-cell model with one Li^+ ion in the electrolyte gradually approaching the Li-metal surface. The full-filled square in **Fig. 4b** is from SCC-DFTB minimization, and the half-filled circle is from SCC-DFTB MD average along with its fluctuation, and unfilled diamond is from GGA/PBE. It is apparent that at this charge density of σ = -0.14 e/nm^2 (predicted by SCC-DFTB), Li^+ ion prefers to be dissolved in the electrolyte and Li-platting will not occur under this potential. A lower potential is needed to plate Li, as discussed in **Section 3.1**. As shown in **Fig. 4b**, the SCC-DFTB calculated energy remains almost unchanged when Li^+ ion diffuses inside the EC electrolyte from 23 to 16 Å toward the Li-metal surface (defines as position 0), consistent with the analytical analysis in **Fig. S2a**. Then, the energy sharply increases as the Li^+ ion approaches the Li_2CO_3 surface at 13.2 Å, where the Li^+ ion is absorbed on the Li_2CO_3 surface, as its bond distance with the O on the surface of Li_2CO_3 is close to the Li-O bond length in the Li_2CO_3 phase. At this desolvated state, two EC molecules were stripped away from the primary solvation sheath $Li^+(EC)_5$ to form $Li^+(EC)_3$. After that, the Li^+ ion continuously transports into the Li_2CO_3 layers by forming an interstitial Li_i^+ in the Li_2CO_3 lattice. The energy decreases as the Li^+ ion gets closer to the Li/Li_2CO_3 interface, due to the electrostatic interaction. DFT result has a similar energy landscape, but with a smaller value.

The energy landscapes at different charge density on the Li-metal electrode were simulated directly by the half-cell model with SCC-DFTB. **Fig. 5** shows the energy landscape for serval oxidized states, corresponding to the charge density of -0.14, -0.28, -0.42, and -0.70 e nm^{-2} on the Li-metal electrode, which correspond to 1, 2, 3 and 5 Li+ ions dissolved in the electrolyte (leading to Li^+ concentration of 0.45, 0.91, 1.36, 1.82, and 2.27 M, respectively). The full-filled symbol is from SCC-DFTB minimization and the half-filled symbol is from SCC-DFTB MD average along with its fluctuation. All the reduced state (at the RC of 0 Å) refer to the same state as shown in Fig 1a. Their energies are shifted to show the energy difference between the reduced state and the oxidized state as the negative charge density on Li-metal electrode changes from -0.14 to -0.70 e

nm^{-2}. This is the thermodynamic driving force for the reduction reaction shown in **Fig. 2**. This indicates that Li atoms are continuously stripped from the neutral Li-metal electrode, dissolved as Li^+ ion into the electrolyte and leaving negative charges on the Li-metal electrode, until a balance of the energies between the oxidized and reduced state is achieved. The buildup of excess electrons on the Li-metal surface and higher concentration of Li^+ ion near the surface can be established especially due to the ionic conductive and electronically insulating properly of the SEI layer.

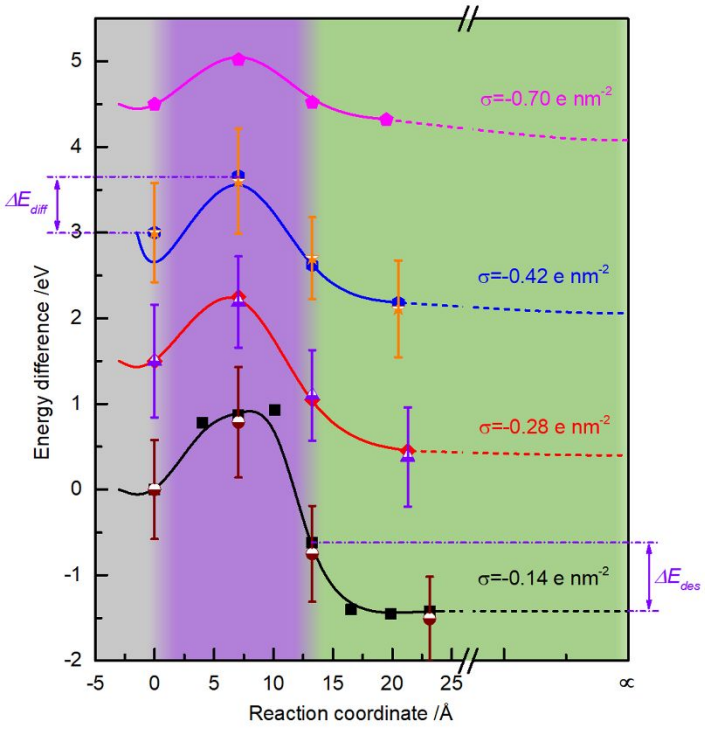

Fig. 5 Energetic coordinates for Li^+ ion transport as a function of charge density on the Li-metal surface via the Li/Li_2CO_3/EC interface model. The half-filled symbol is from SCC-DFTB MD average along with its fluctuation, the full-filled symbol is from SCC-DFTB minimization. The desolvation barrier and the transport energy barrier through SEI are defined by the energy landscape.

The energy landscape indicates two energy barriers for Li^+ ion transport, the de-solvation energy barrier from the electrolyte to the surface of Li_2CO_3, and the diffusion barrier inside the

Li_2CO_3. The de-solvated state is already inside the inner Helmholtz layer in the EDL model. The charge on the Li-metal will change the double layer thickness. The energy landscape at σ=0.14 e nm^{-2} shows that the energy of the system is converged in the center of the electrolyte (RC from 20~25 Å), where the bulk electrolyte concentration is reached. However, due to the size limitation of the simulation cell, the increase of Li^+ ion concentration in electrolyte results in the primary solvation sheath changing from $Li^+(EC)_5$ to $Li^+(EC)_4$ as at σ becomes more negative to -0.7 e nm^{-2}. Meanwhile, the average Li^+-O bond length in the solvation sheath increased from 1.927 Å to 1.987 Å, suggesting the solvation sheath $Li^+(EC)_5$ already begins de-solvation at a distance of ~10 Å from the Li_2CO_3/EC-electrolyte interface under the electric field caused by the more negative charge density (-0.70 e nm^{-2}) on the Li-metal electrode. However, the bulk solvation sheath far away from this interface should remain a constant out of the outer Helmholtz plane, beyond which the Li^+ ion concentration is unchanged. Therefore, the energy of the oxidized states with Li^+ ions in bulk electrolyte, E_{bulk}(oxi), is extrapolation by subtracting the energy difference (ΔE_{sol}) induced by Li^+ ion concentration (seen in **Fig. S4**). The de-solvation barrier is then defined by $\Delta E_{des}=E_{surf}(oxi)- E_{bulk}(oxi)$. The energy landscape at σ=0.14 e nm^{-2} shows that the migration of Li^+ ion inside the Li_2CO_3 layer is driven by the electric field, as the total energy decreases at the Li^+ ion moves closer to the Li/Li_2CO_3 interface. The electric potential $\phi(x)$ drops through the Li_2CO_3 layer (1.2 nm) estimated from the classical model is ~0.3 eV (show in **Fig. S2**). This is consistent with the ~0.1 eV drop as Li^+ ion travels ~0.6 nm distance inside the Li_2CO_3 layer. (also shown in the SCC-DFTB data in **Fig. 4b**). The energy change inside the Li_2CO_3 was not calculated for other σ values. We simply took the energy of the Li^+ ion in the middle of the Li_2CO_3 layer and define its difference with respect to the reduced state as the Li^+ ion transport barrier through the SEI as $\Delta E_{diff}=E(SEI)- E_{surf}(red)$ **(Fig. 5).**

3.5 Desolvation Energy Barrier and the EDL Structure

Fig. 6a shows the desolvation barrier obtained from **Fig 5**. The desolvation energy barrier decreases with a more negative charge density on the Li electrode. Around the electrochemical equilibrium potential or the experimentally defined zero-volt for Li^+/Li^0, the desolvation barrier is about 0.49 ± 0.04 eV within the range of charge density corresponding to the equilibrium state, corresponding to charge density of 0.62 ± 0.12 e nm^{-2}. This barrier is comparable to the

experiment activation energies of ~0.5 eV at an SEI covered graphite/EC:DMC electrolyte interface.[27, 28, 51]

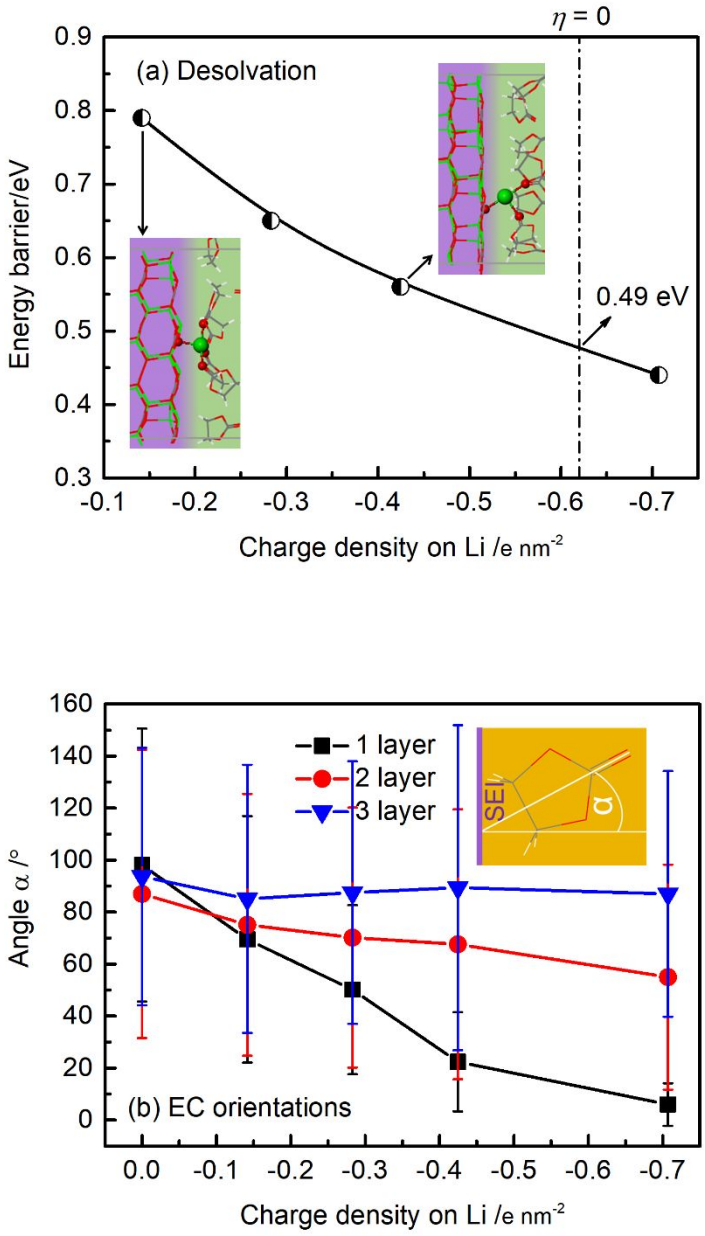

Fig. 6. (a) Desolvation barriers on EC electrolyte surface at Li/Li_2CO_3/EC interface as a function of charge density on the Li-metal electrode, and (b) the orientations of EC relative to the SEI surface under different charge density on Li electrode. Layer 1, 2, and 3 are 4 Å thick regions in parallel to the Li_2CO_3 surface, arranged in the sequence from closer to far away from the surface.

At the desolvated state, the solvation sheath changed from $Li^+(EC)_3$ to $Li^+(EC)_2$ (**Fig. 6a** inserts) with a more negative charge density on the Li-metal electrode. This is because the strong electric filed leads to a preferential orientation for the interfacial EC solvents, with their C=O carbonyl groups point away from the interface. In order to clarify the effects of the electric field on the solvation sheath or the double layer structure near the Li_2CO_3/EC-electrolyte interface, the orientation of EC solvent molecules was quantified as the angle ($0^\circ \leq \alpha \leq 180^\circ$) between the C=O bond direction and the normal of the Li_2CO_3/EC-electrolyte interface. The angle close to 0° indicates that C=O bonds point away and from the interface. On the contrary, the angle close to 90° with large standard deviation indicates that C=O bonds are randomly orientated. The orientation angle distribution of the EC molecules within different regions away from the interface, named as "1 layer", "2 layer", and "3 layer", were analyzed as shown in **Fig. 6b and Table S-1 in the SI.** More specifically, layer 1 is a 4 Å region next to Li_2CO_3|EC-electrolyte interface, layer 2 and layer 3 are 8 Å, and 12 Å further away from the Li_2CO_3|EC-electrolyte interface. At neutral and low electron density (σ= 0 and -0.14 e nm^{-2}) the average C=O bond direction angle of all EC molecules in the three layers are closed to $90\pm50^\circ$ indicating all EC molecules are in random distribution. At a more negatively charged surface (especially at σ= -0.70 e nm^{-2}), the EC molecules in layers 1 and 2 show a strong preference for the C=O carbonyl group to point away from the SEI surface, indicated by their reduced angle and standard deviation. The ordering in layer 1 clearly increases with the more negative charge on Li-metal, as the deviation drops from 52.5° at σ= 0 to 8.0° at σ= -0.70. This preference is attributed to the strong electric field interaction. In the electrolyte far away from the interface, namely layer 3, the EC molecules were found to be essentially randomly oriented, consistent to the zero potential in the center of the electrolyte shown in **Fig S2a.**

Therefore, the stronger electric field introduces two contributions to the desolvation barrier. One is the Coulombic interaction between Li^+ ion and the negative potential, resulting in lower E_{surf}(oxi) thus the reduction of the desolvation barrier. On the other hand, the stronger electric field tends to align the EC solvents into an ordered structure on the surface of Li_2CO_3. The Li^+ ion bonded C=O carbonyl groups must rotate to allow the Li^+ ion to be absorbed on the Li_2CO_3 surface, one more EC was lost from the solvation sheath under the stronger negative electric field. This causes an increase of the desolvation energy barrier. Obviously, the former effect dominates, thus desolvation barrier decreases on the more negatively charged Li-metal electrode.

3.6 Li^+ Ion Transport through the SEI Layer

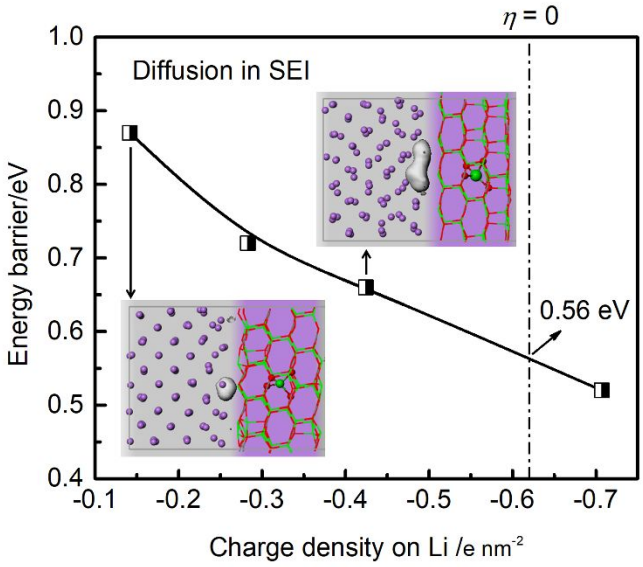

Fig. 7 The energy barriers of a Li^+ ion to form and transport in the Li_2CO_3 at the Li/Li_2CO_3/EC interface as a function of charge density on the Li-metal electrode.

Fig. 7 shows the Li^+ ion transport energy barrier in Li_2CO_3 lattice obtained from the energy landscape in **Fig 5**. Note the transport of Li^+ ion in a Li_2CO_3 lattice is limited by the concentration of Li^+ ion interstitials, as its formation energy (depends on Li chemical potential) is much larger than its diffusion barrier. In Li_2CO_3, the DFT predicted defect formation energy, in equilibrium with Li-metal, is ~0.5 eV and the diffusion barrier is ~0.3 eV.[52, 53] The current model only captured the stable structure with Li^+ ion on the interstitial sites, not the diffusion barrier. So **Fig. 7** means the formation energy of the interstitial Li_i^+ in Li_2CO_3 layers (E_f) is about 0.80-0.90 eV at σ=-0.14 e nm^{-2}. The formation energy of Li^+ ion in Li_2CO_3 decreased with the more negative charges on the Li-metal, due to Coulombic interaction as shown in **Fig. 7**. The E_f is about 0.56 eV at zero voltage, which is consistent with that from DFT.[52, 53] The diffusion energy barrier of Li^+ ion in Li_2CO_3 at zero voltage can be estimated as the summation of the formation energy and diffusion barrier, or $E_f + E_m = 0.56+0.30=0.86$ eV, which is slightly larger than that at graphite electrode of the 0.66 eV value from electrochemical impedance spectroscopy measurements.[21] This relatively

high energy barrier might is due to the use of the perfect crystalline Li_2CO_3. If there are existing interstitials, Li^+ ion transport may not be limited by its formation energy anymore.

From the energy landscape, it seems that Li^+ ion needs to desolvate then transport through the interstitial sites in Li_2CO_3 before it annihilates with the electron. Under the current framework, it can be seen the Li^+ ion transport through the SEI is the rate-limiting step. As the current model used a perfect Li_2CO_3 crystal representing the SEI, it ignored the heterogeneity and any defects in the SEI. The defective Li_2CO_3 at room temperature may have a much-reduced diffusion barrier [51].

3.7 Derived the Charge Transfer Coefficient Based on the Computed Energy Landscape

Overall the variation of the energy landscape with the over potential η can lead to a direct estimation of the charge transfer coefficient, α, in the Bulter-Volmer equation. The top curve in **Fig. 5** signifies the equilibrium condition, where $\eta = 0$. The decrease of the excess electrons on the Li-metal electrode, leads to depletion of Li with $\eta > 0$. One can assume a linear relationship between ϕ and σ. Then $\alpha = \frac{\partial E_a}{\partial \phi}$, where E_a is the energy barrier for the overall charge transfer reaction. When σ = -0.14 e nm^{-2}, the over-potential $\eta \sim 1.4\,V$, the energy barrier is ~0.87 eV, it dropped to 0.56 eV at the equilibrium $\eta = 0$. Thus, it is estimated that $\alpha \sim 0.22$. This means the Bulter-Volumer equation is

$$i = i_f - i_b = i_0\left[\exp\left(\frac{0.22F\eta}{RT}\right) - \exp\left(\frac{0.78F\eta}{RT}\right)\right]. \quad (9)$$

Thus the Li charge transfer reaction is not symmetric. On the other hand, it means, the energy barrier is lowered more during delithiation than lithiation. This is consistent with the energy barrier measurements that gave the unsymmetrical property of Li^+ ion cells of fast discharging but slow charging [25-27]. This is also consistent with the polarized curve measurements that gave α varying from 0.11 for pure DMC to 0.24 for pure PC. [3]

4. Conclusions

In summary, the modeling revealed many details for the charge transfer reaction at the Li/Li_2CO_3/EC-electrolyte interface. First, it is important to note the zero-volt for Li^+/Li^0 does not occur on a zero-charged Li-metal electrode. The reaction energy shows that Li^+ ion is much more energetically favorable to be dissolved in the electrolyte on a zero-charged Li-metal electrode,

indicating the SEI is a necessary kinetic barrier to prevent complete solvation of Li-metal into the electrolyte. At the electrochemical equilibrium or the experimentally defined zero-voltage for Li^+/Li^0, the Li-metal surface is negatively charged ($\sim 0.62 \pm 0.12$ e nm^{-2}). During delithiation, Li^+ ion would be stripped from the surface non-uniformly and form a large void on the Li-metal surface, suggesting the need for a compressive stress to avoid SEI delamination. During lithiation, it was demonstrated the annihilation of Li^+ ion and electron is at the Li/SEI interface, for an idealized defect free SEI. The overall Li^+ ion desolvation energy barrier decreases with the negative charge density on the Li-metal surface. At the voltage of Li-plating, the electric field orients the EC electrolyte molecules into an ordered surface structure. The Li^+ ion transport in the SEI is limited by the formation of Li^+ ion interstitials in crystalline Li_2CO_3, and the negative charge density decreases the formation energy the Li^+ ion interstitials, thus helps the Li^+ ion transport through the SEI. Further, the charge transfer coefficient, α, in the Butler-Volmer equation was directly predicted from the computed energy landscape. A nonsymmetric α~0.22 is predicted, consistent with the experimental measurements. Thus, this model enables a bottom-up multiscale modeling approach for ion-transfer electrochemical reactions.

Acknowledgment

We acknowledge the support from the Department of Energy, Office of Energy Efficiency and Renewable Energy (EERE), under the Awards #DE-EE0007787 and #DE-EE0007803. The authors especially thank Drs Kevin Leung, Long-Qing Chen, Xingcheng Xiao, Mark Verbrugge, and Michael Swift for constructive suggestions.

References

1. L. Liang, Y. Qi, F. Xue, S. Bhattacharya, S. J. Harris and L.-Q. Chen, *Phys. Rev. E*, 2012, **86**, 051609.
2. A. M. Liu, X. F. Ren, M. Z. An, J. Q. Zhang, P. X. Yang, B. Wang, Y. M. Zhu and C. Wang, *Sci. Rep.*, 2014, **4**.
3. O. Crowther and A. C. West, *J. Electrochem. Soc.*, 2008, **155**, A806-A811.
4. R. Bhattacharyya, B. Key, H. Chen, A. S. Best, A. F. Hollenkamp and C. P. Grey, *Nat. Mater.*, 2010, **9**, 504.
5. D. Aurbach, E. Zinigrad, H. Teller and P. Dan, *J. Electrochem. Soc.*, 2000, **147**, 1274-1279.
6. C. D. Taylor, *Int. J. Corros.*, 2012, **2012**, 13.
7. P. Bai and M. Z. Bazant, *Nat. Commun.*, 2014, **5**, 3585.
8. C. Monroe and J. Newman, *J. Electrochem. Soc.*, 2004, **151**, A880-A886.
9. W. Schmickler, *Interfacial Electrochemistry*, OXFORD UNIVERSITY PRESS, New York, 1996.
10. R. Sundararaman, W. A. GoddardIII and T. A. Arias, *J. Chem. Phys.*, 2017, **146**, 114104.
11. R. Sundararaman and K. Schwarz, *J. Chem. Phys.*, 2017, **146**, 084111-084111.
12. C. D. Taylor, S. A. Wasileski, J.-S. Filhol and M. Neurock, *Phys. Rev. B*, 2006, **73**, 165402.
13. M. B. Goldey, N. P. Brawand, M. Vörös and G. Galli, *J. Chem. Theory Comput.*, 2017, **13**, 2581-2590.
14. F. Calle-Vallejo and M. T. M. Koper, *Electrochim. Acta*, 2012, **84**, 3-11.
15. J. D. Goodpaster, A. T. Bell and M. Head-Gordon, *J. Phys. Chem. Lett.*, 2016, **7**, 1471-1477.
16. L. D. Chen, M. Urushihara, K. Chan and J. K. Nørskov, *ACS Catal.*, 2016, **6**, 7133-7139.
17. T. A. Pham, X. Zhang, B. C. Wood, D. Prendergast, S. Ptasinska and T. Ogitsu, *J. Phys. Chem. Lett.*, 2018, **9**, 194-203.
18. K. Xu, *Chem. Rev.*, 2004, **104**, 4303-4418.
19. K. Xu, *Chem. Rev.*, 2014, **114**, 11503-11618.
20. Y. Li, K. Leung and Y. Qi, *Acc. Chem. Res.*, 2016, **49**, 2363-2370.
21. H. Schranzhofer, J. Bugajski, H. J. Santner, C. Korepp, K. C. Möller, J. O. Besenhard, M. Winter and W. Sitte, *J. Power Sources*, 2006, **153**, 391-395.

22. K. Leung, Y. Qi, K. R. Zavadil, Y. S. Jung, A. C. Dillon, A. S. Cavanagh, S.-H. Lee and S. M. George, *J. Am. Chem. Soc.*, 2011, **133**, 14741-14754.
23. A. Wang, S. Kadam, H. Li, S. Shi and Y. Qi, *npj Comput. Mater.*, 2018, **4**, 15.
24. K. Leung and C. M. Tenney, *J. Phys. Chem. C*, 2013, **117**, 24224-24235.
25. T. Abe, H. Fukuda, Y. Iriyama and Z. Ogumi, *J. Electrochem. Soc.*, 2004, **151**, A1120-A1123.
26. T. Abe, F. Sagane, M. Ohtsuka, Y. Iriyama and Z. Ogumi, *J. Electrochem. Soc.*, 2005, **152**, A2151-A2154.
27. Y. Yamada, Y. Iriyama, T. Abe and Z. Ogumi, *Langmuir*, 2009, **25**, 12766-12770.
28. K. Xu, A. von Cresce and U. Lee, *Langmuir*, 2010, **26**, 11538-11543.
29. M. Elstner, D. Porezag, G. Jungnickel, J. Elsner, M. Haugk, T. Frauenheim, S. Suhai and G. Seifert, *Phys. Rev. B*, 1998, **58**, 7260-7268.
30. T. Frauenheim, G. Seifert, M. Elstner, T. Niehaus, C. Kohler, M. Amkreutz, M. Sternberg, Z. Hajnal, A. Di Carlo and S. Suhai, *J. Phys.: Condens. Matter*, 2002, **14**, 3015-3047.
31. Y. Li and Y. Qi, *J. Phys. Chem. C*, 2018, **122**, 10755-10764.
32. K. Leung, *Phys. Chem. Chem. Phys.*, 2015, **17**, 1637-1643.
33. I. Abou Hamad, M. A. Novotny, D. O. Wipf and P. A. Rikvold, *Phys. Chem. Chem. Phys.*, 2010, **12**, 2740-2743.
34. R. Jorn, R. Kumar, D. P. Abraham and G. A. Voth, *J. Phys. Chem. C*, 2013, **117**, 3747-3761.
35. S. Dewan, V. Carnevale, A. Bankura, A. Eftekhari-Bafrooei, G. Fiorin, M. L. Klein and E. Borguet, *Langmuir*, 2014, **30**, 8056-8065.
36. W. Tang, E. Sanville and G. Henkelman, *J. Phys.: Condens. Matter*, 2009, **21**, 084204.
37. K. F. Young and H. P. R. Frederikse, *J. Phys. Chem. Ref. Data*, 1973, **2**, 313-410.
38. D. S. Hall, J. Self and J. R. Dahn, *J. Phys. Chem. C*, 2015, **119**, 22322-22330.
39. Zhang, Y.; Evans, J. R. G.; Yang, S., *J. Chem. & Eng. Data* 2011, 56, 328-337.40. Moore, C. E., National Standard Reference Data Series. Washington, DC, 1970; Vol. 34.
41. I. Skarmoutsos, V. Ponnuchamy, V. Vetere and S. Mossa, *J. Phys. Chem. C*, 2015, **119**, 4502-4515.
42. S. Yanase and T. Oi, *J. Nucl. Sci. Technol.*, 2002, **39**, 1060-1064.

43. K. Kokko, P. T. Salo, R. Laihia and K. Mansikka, *Surf Sci.*, 1996, **348**, 168-174.
44. Y.-X. Lin, Z. Liu, K. Leung, L.-Q. Chen, P. Lu and Y. Qi, *J. Power Sources*, 2016, **309**, 221-230.
45. Y. Wang, S. Nakamura, M. Ue and P. B. Balbuena, *J. Am. Chem. Soc.*, 2001, **123**, 11708-11718.
46. S. Trasatti, *Pure Appl. Chem.*, 1986, **58**, 955-966.
47. P. Koskinen and V. Mäkinen, *Comput. Mater. Sci.*, 2009, **47**, 237-253.
48. D. Lin, Y. Liu and Y. Cui, *Nature Nanotechnology*, 2017, **12**, 194.
49. Z. Liu, Y. Qi, Y. X. Lin, L. Chen, P. Lu and L. Q. Chen, *J. Electrochem. Soc.*, 2016, **163**, A592-A598.
50. K. R. Z. Katharine L. Harrison, Nathan T. Hahn, Xiangbo Meng, Jeffrey W. Elam, Andrew Leenheer, Ji-Guang Zhang, Katherine L. Jungjohann, *ACS Nano*, 2017, **11**, 11194-11205.
51. K. Xu and A. von Cresce, *J. Mater. Chem.*, 2011, **21**, 9849-9864.
52. S. Shi, P. Lu, Z. Liu, Y. Qi, L. G. Hector, H. Li and S. J. Harris, *J. Am. Chem. Soc.*, 2012, **134**, 15476-15487.
53. S. Shi, Y. Qi, H. Li and L. G. Hector, *J. Phys. Chem. C*, 2013, **117**, 8579-8593.

Electrochemical reactions, occurring at the interface between a solid electrode and a liquid electrolyte, hold the key to designing energy conversion and storage technologies. However, considerable gaps remain in the fundamental understanding of the charge transfer pathways on a non-pristine metal surface, which is common for real-world applications. The Li-metal electrode, promising high energy density rechargeable batteries, amplifies the challenge as the Li-metal electrode is always covered by a layer of solid electrolyte interphase (SEI). This article develops a half-cell model based on the Li/SEI/electrolyte interface in order to compute the charge transfer reaction energy landscape with quantum precision. The new model showed the charge transfer reaction occurs at the Li/SEI interface if the SEI is ideal. It further showed the Li-metal surface is negatively charged most of the time during lithiation and delithiation. The negatively charged surface has a profound impact on the electrolyte structure and the charge transfer reaction kinetics. Finally quantifying the energy landscape under different potential leads to a directly computed charge transfer coefficient used in the Butler-Volmer equation, which is typically obtained through fitting experiments. In summary, this method enables a bottom-up multiscale modeling approach for ion-transfer electrochemical reactions.